Received: 24 September 2020 | Revised: 26 November 2020 | Accepted: 6 December 2020

DOI: 10.1002/htj.22033

RESEARCH ARTICLE

HEAT TRANSFER WILEY

Nonlinear convection flow of dissipative Casson nanofluid through an inclined annular microchannel with a porous medium

Amos S. Idowu | **Mojeed T. Akolade** | **Timothy L. Oyekunle** | **Jos U. Abubakar**

Department of Mathematics, Faculty of Physical Sciences, University of Ilorin, Ilorin, Nigeria

Correspondence
Mojeed T. Akolade, Department of Mathematics, Faculty of Physical Sciences, University of Ilorin, Ilorin 240003, Nigeria.
Email: 17-68ev006pg@students.unilorin.edu.ng

Abstract

The nonlinear convection study on the flow of a dissipative Casson nanofluid through a porous medium of an inclined micro-annular channel is presented. The cylindrical surfaces were conditioned to temperature increase and velocity slip effects. A uniform magnetic field strength was applied perpendicular to the cylinder surface. The heat source and Darcy number influence are explored in the examination of the blood rheological model (Casson) through the annular cylinder. Appropriate dimensionless variables are imposed on the dimensional equations encompassing Casson nanofluid rheology through an annular microchannel. The resulting systems of equations were solved and computed numerically via Chebyshev-based collocation approach. Thus, the solutions of flow distributions, volumetric flow rate, and other flow characteristics were obtained. The result shows that both nonlinear convection parameters decrease the nanoparticle volume fraction, whereas they increase the energy and momentum distributions. Moreover, the volumetric flow rate is upsurged significantly by a wider porous medium, annular gap, a higher Casson parameter, and nonlinear convection influence.

KEYWORDS

annular channel, Casson fluid, Chebyshev collocation method, MHD, nanofluid, nonlinear convection

 © 2020 Wiley Periodicals LLC

1 | INTRODUCTION

The study of convection flow process, heat, and mass transfer in a non-Newtonian fluid (Casson nanofluid) with a porous medium is of practical importance due to their applications in industries, engineering, and power stations of numerous design characteristics where cooling/heating is required. These include filtration processes, warm protection, cooling electronic hardware, groundwater, storage of oil and gas, nuclear wastes, heat pipes, prevention of systems from overheating, improvement of household appliances, technology advancements, electronics, among others. Thus, to achieve any remarkable convection process, an increase in the material thermal conductivity would be required for accurate prediction of heat and mass transfer across the flow region. Considering the real impact of convection on the flow process, it is imperative to examine the effect of porosity, magnetic field, heat generation, and slip and jump impact on the movement of a Casson nanofluid through a microchannel.

In mechanical procedures, porous medium and nanofluid are considered the best combination for effective convection heat and mass transfer.[1] Concerning this, several attempts have been made to seek better performance in mechanical industries. Thus, Sankar and Makinde[2] modeled the buoyant convection in porous media, Lawal and Jibril[3] analyzed the time-dependent MHD convective flow of ramped motion in an annulus medium, and Panigrahi et al.[4] investigated the fully developed flow of a polar fluid in concentric annuli with a radial magnetic field influence. Anurag et al.[5] presented the cooling/heating effect on an annular permeable region, where Newtonian heating is seen to enhance both momentum and energy field, accordingly. Recently, a series of investigations of convective flow in a vertical annular porous medium have been carried out. Jha et al.,[6] Oni and Jha,[7] Jha et al.,[8] Yusuf,[9] and Jah and Yusuf[10] analyzed the transient free convective flow through the porous material; Isa et al.[11] observed the steady-state flow regime and time-periodic boundary conditions through a vertical microcircular duct; and recently, Gireesha and Sindhu[12] performed the analysis on the heat absorption/generation of a Casson fluid flow through the annular microchannel. They established that a higher magnitude of Casson and Hartmann's number decelerates the fluid momentum, and that the heat-generating parameter predicts the skin friction positively.

The nonlinear convection flow has gained an immense interest owing to its extensive range of applications in engineering, geophysics, and industrial manufacturing process. Considering these numerous applications, researchers like Thriveni et al.[13] and Mahanthesh et al.[14] discussed the effectiveness and significance of induced MHD of nanoparticles in thermal convective transport of the Casson fluid. Pantzali et al.[15] experimentally addressed the significance of Cu–water nanoparticles on the surface of heat exchangers. Hamad et al.[16] presented the nonlinear convection flow analysis of a laminar flow of a viscous liquid through a porous medium filled with nanoparticles, whereas Pal and Mandal[17] analyzed the combined effects of convection and viscous heating on the nanofluid flow. Gyatri et al.[18] investigated the features of the Maxwell fluid flow through a stretching sheet with a heat source/sink. It was discovered that nonlinear convection enriches both the energy and velocity profile, whereas it decreases the concentration field. Kumar and Sood[19] analyzed the combined effect of nonlinear convection and magnetic field on the stagnation point flow over a shrinking sheet. It is found that the nonlinear convection and magnetic field parameters enhanced the solution range.

Concerning the nonlinear convective flow, Thriveni and Mahanthesh[20,21] investigated the magnetohybrid nanoliquid flow with radiative and nonlinear buoyancy effects in an

annulus channel, which was the first study on the statistical framework, and later on, they carried out sensitivity analysis and optimization of heat transport. The MHD Jeffrey nanofluid flow over a nonlinear stretching sheet was analyzed by Hayat et al.[22] The study of the Williamson nanofluid flow past a radially stretching surface was carried out by Wubshet and Dachasa.[23] It was observed that the velocity profile enhanced as the values of nonlinear convection upgraded. Adesanya et al.[24] analyzed the flow of a reactive couple stress fluid with entropy generation through a channel filled with saturated materials and subject to convective cooling. They discovered that a hike in both linear and nonlinear convective parameters enhanced the velocity and temperature profiles but depleted the energy of the system. The MHD Oldroyd 8-constant fluid flow between vertical plates with chemical reaction was examined by Yusuf et al.,[25] who revealed that enhancement in magnetic field strength undermines the flow velocity, temperature, and concentration. The flow of a hyperbolic tangent fluid with the Cattaneo–Christov heat and mass diffusion through a stretching surface was reported by Ibrahim and Gizewu.[26] Hayat et al.[27] presented the salient feature analysis on the flow of a thixotropic fluid in the version of the Cattaneo–Christov heat flux theory. They discovered that higher values of mixed convection parameter lead to a decrease in the fluid temperature and boundary layer thickness. The study of the nonlinear convective flow of a non-Newtonian fluid over an inclined plate with the convective surface condition was carried out by RamReddy et al.,[28] whereas Hayat et al.[29] analyzed the MHD nonlinear convective flow of Walter's B nanofluid. It is concluded that the thermal field and heat transfer rate are enhanced with an increase in the temperature ratio parameter.

Idowu et al.[30] and Alamri et al.[31] presented the novel study of MHD with modified Fourier law on a Casson dissipative fluid and flow of second-grade fluid, respectively. Elelamy et al.[32] investigated the MHD blood flow rheology subjected to slip and heat transfer effects. Bhatti et al.[33] analyzed the magnetized motile movement of a nanofluid past a porous plate with activation energy, and Akolade et al.[34] examined the MHD squeezed flow of a Casson dissipative fluid with variable properties. The influence of the transverse magnetic field in an inclined microporous channel was investigated by Aina and Malgwi.[35] It is realized that an increase in the inclination angle yields an enhancement in fluid velocity within the microporous channel. Yusuf et al.[36] also presented the influence of MHD flow of a Williamson nanofluid over a stretching sheet with chemical reaction. They reported that the rate of mass transferred may be maximum with the variation of Williamson and chemical reaction parameters. Srinivasacharya and Bindu[37] presented the entropy generation in a micropolar fluid flow through an inclined channel. The result reveals that the entropy generation number increases with the inclination angle. Other researchers dealing with an inclined microchannel include Shiriny et al.[38] and Gireesha and Roja.[39] They also observed a higher magnitude of velocity and temperature with an increase in the inclination angle.

The literature analysis reveals that studies on the nonlinear convection flow of a dissipative Casson nanofluid through an inclined annular microchannel with a porous medium have not been reported yet. The present study of the blood rheology (Casson fluid) with nanoparticles is experimented through an inclined annular microchannel with a porous medium. The objectives are to simulate and investigate the combined effects of thermophoresis, Brownian motion, radii ratio, nonlinear thermal and solutal convection, inclination angle parameters, among others, and illustrate the Chebyshev-based collocation approach (CCA) for the nonlinear convection flow of a dissipative Casson nanofluid through the annular porous medium.

2 | PHYSICAL MODEL FORMULATION

The fully developed nonlinear convection flow of a Casson nanofluid through an inclined annular porous microchannel is considered. The steady, incompressible, and electrically conducting Casson nanoparticle fluid flow process is subjected to the magnetic field strength (B_0). The inclined cylindrical surfaces are conditioned to temperature increase and velocity slip effects. The outer and inner cylinders are at temperature V_2 and V_1, and nanoparticle volume fraction W_2 and W_1, respectively. In Figure 1, the microchannel is at an angle γ. The r-axis is considered toward the flow direction, whereas the t-axis is taken perpendicular to it, and c_2 and c_1 are the cylinder's outer and inner radius, respectively. The governing equations comprising continuity, momentum, energy, and concentration equations for the magnetized Casson nanofluid are as follows:

$$\nabla \cdot U = 0, \tag{1}$$

$$\rho_f([U \cdot \nabla]U) = -\nabla P + \mu\nabla^2 U - \rho_K g \cos[\gamma] + J \times B_0 - \frac{\mu}{k_p}U, \tag{2}$$

$$\rho_f c_p([U \cdot \nabla]V) = \kappa\nabla^2 V + \tau\left[D^*\nabla V \cdot \nabla W + \left(\frac{D_a}{V_0}\right)\nabla V \cdot \nabla V\right] + \mu(\nabla U \cdot \nabla U) + Q, \tag{3}$$

$$[U \cdot \nabla]W = D^*\nabla^2 W + \left(\frac{D_a}{V_0}\right)\nabla^2 V. \tag{4}$$

The kinematic viscosity (ν) depends on the fluid density (ρ), dynamic viscosity (μ), and Casson parameter (β), which is given as follows[30,34]:

$$\nu = \frac{\mu}{\rho}\left(1 + \frac{1}{\beta}\right). \tag{5}$$

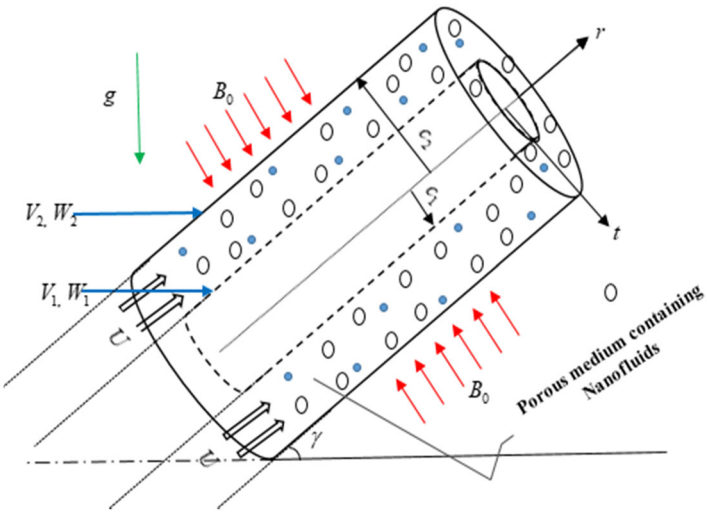


FIGURE 1 The physical coordinate system of the model [Color figure can be viewed at wileyonlinelibrary.com]

The current density $J = -\sigma_0(E + U \times B_0)$, where $E = 0$ (i.e., no external electric field), $Q = Q^*(V - V_0)$ denotes the heat source/sink influence, and the buoyancy force $\rho_K = -[k_0(V - V_0) + k_1(V - V_0)^2 + j_0(W - W_0) + j_1(W - W_0)^2]$ represents the suitable non-linear and linear thermal and solutal convection process.

Under the assumptions of constant fluid properties, steady state, absence of pressure, and external electric field, for isentropic and incompressible Casson fluid, the governing systems of fully developed, MHD, electrically conducting nanofluid fluid flow through an inclined porous medium are as follows[8,24,39]:

$$\left(1 + \frac{1}{\beta}\right)\frac{\nu}{t}\frac{d}{dt}\left[t\frac{dU}{dt}\right] + g\cos\gamma[k_0(V - V_0) + k_1(V - V_0)^2 + j_0(W - W_0) + j_1(W - W_0)^2] - \left[\frac{\sigma_0 B_0^2}{\rho_f} + \frac{\nu}{k_p}\left(1 + \frac{1}{\beta}\right)\right]U = 0, \tag{6}$$

$$\frac{\alpha^*}{t}\frac{d}{dt}\left[t\frac{dV}{dt}\right] + \left(1 + \frac{1}{\beta}\right)\frac{\nu}{\rho_f c_p}\left(\frac{dU}{dt}\right)^2 + \frac{Q^*}{\rho_f c_p}(V - V_0) + \tau\left[D^*\frac{dW}{dt}\frac{dV}{dt} + \frac{D_a}{V_0}\left(\frac{dV}{dt}\right)^2\right] = 0, \tag{7}$$

$$\frac{D^*}{t}\frac{d}{dt}\left[t\frac{dW}{dt}\right] + \frac{D_a}{V_0}\frac{d^2V}{dt^2} = 0, \tag{8}$$

subjected to the boundary conditions:

$$\begin{aligned} U(t) &= \left(1 + \tfrac{1}{\beta}\right)\beta_v\varsigma_d\frac{dU(t)}{dt}, V(t) - V_1 = h_t\frac{2\gamma_a}{\gamma_a + 1}\frac{\varsigma_d}{Pr}\frac{dV(t)}{dt}, W(t) = W_1, \text{at} t = c_1, \\ U(t) &= -\left(1 + \tfrac{1}{\beta}\right)\beta_v\varsigma_d\frac{dU(t)}{dt}, V(t) - V_2 = -h_t\frac{2\gamma_a}{\gamma_a + 1}\frac{\varsigma_d}{Pr}\frac{dV(t)}{dt}, W(t) = W_2, \text{at} t = c_2, \end{aligned} \tag{9}$$

where $\beta_v = \frac{2-\sigma_v}{\sigma_v}$, $h_t = \frac{2-\sigma_t}{\sigma_t}$, $\tau = \frac{(\rho c)_p}{(\rho c)_f}$, $\alpha^* = \frac{\kappa^*}{\rho_f c_p}$, $\varsigma_d = \frac{\sqrt{\pi R V_0 / 2\mu}}{\rho_f}$.

Introducing the given dimensionless variables in equation (10) on the governing Equations (6)–(9),

$$\xi = \frac{t - c_1}{\delta}, \delta = c_2 - c_1, u = -\frac{U}{\lambda_m}, \eta = \frac{c_1}{c_2}, \lambda_m = \frac{\rho_0 g k_0 (V_1 - V_0)}{\mu_0}\delta^2, v = \frac{V - V_0}{V_1 - V_0}, \quad w = \frac{W - W_0}{W_1 - W_0}. \tag{10}$$

The governing systems of Equations (6)–(9) are reduced to the following:

$$\left(1 + \frac{1}{\beta}\right)\frac{1}{\phi(\xi)}\frac{d}{d\xi}\left[\phi(\xi)\frac{du}{d\xi}\right] + \cos[\gamma](v + s_1 v^2 + w + s_2 w^2) - \left\{Ha^2 + \frac{1}{Da}\left(1 + \frac{1}{\beta}\right)\right\}u = 0, \tag{11}$$

$$\frac{1}{\phi(\xi)}\frac{d}{d\xi}\left[\phi(\xi)\frac{dv}{d\xi}\right] + Pr\left\{\alpha v + Ec\left(1 + \frac{1}{\beta}\right)\left(\frac{du}{d\xi}\right)^2 + Nb\frac{dw}{d\xi}\frac{dv}{d\xi} + Nt\frac{dv}{d\xi}\frac{dv}{d\xi}\right\} = 0, \tag{12}$$

$$\frac{1}{\phi(\xi)}\frac{d}{d\xi}\left[\phi(\xi)\frac{dw}{d\xi}\right]+\frac{Nt}{Nb}\frac{d^2v}{d\xi^2}=0, \tag{13}$$

where as boundary conditions become

$$\begin{aligned} u(\xi)&=\left(1+\tfrac{1}{\beta}\right)\beta_v kn\frac{du}{d\xi}, v(\xi)=1+S\beta_v kn\frac{dv}{d\xi}, w(\xi)=1, \text{at } \xi=0,\\ u(\xi)&=-\left(1+\tfrac{1}{\beta}\right)\beta_v kn\frac{du}{d\xi}, v(\xi)=-S\beta_v kn\frac{dv}{d\xi}, w(\xi)=Rc, \text{at } \xi=1. \end{aligned} \tag{14}$$

Here,

$$\left.\begin{aligned} &\phi(\xi)=[\eta+(1-\eta)\xi], Ha=B_0\eta\sqrt{\tfrac{\sigma_0}{\rho_0\nu}}, Nc=\tfrac{j_0(W_1-W_0)}{k_0(V_1-V_0)}, s_1=(V_1-V_0)\tfrac{k_1}{k_0},\\ &Rc=\tfrac{W_2-W_1}{W_1-W_0}, \alpha=\tfrac{Q^*}{\mu_0 c_p}\eta^2, S=\tfrac{\beta_t}{\beta_v}, Kn=\tfrac{\varsigma_d}{\eta}, Pr=\tfrac{\upsilon}{\alpha^*}, Da=\tfrac{k_p}{\delta^2}, Nb=\tfrac{\tau D^*(W_1-W_0)}{\alpha^*},\\ &Nt=\tfrac{\tau D_a(V_1-V_0)}{V_0\alpha^*}, s_2=(W_1-W_0)\tfrac{j_1}{j_0}, Ec=\tfrac{g^2k_0^2(V_1-V_0)\delta^4}{\upsilon c_p}, \beta_t=\tfrac{2-\sigma_t}{\sigma_t}\tfrac{2\gamma_a}{\gamma_a+1}\tfrac{1}{Pr}. \end{aligned}\right\} \tag{15}$$

The flow characteristics such as the volumetric flow rate

$$Q(\xi)=2\pi\int_0^1 \xi u(\xi)d\xi, \tag{16}$$

the skin-friction (τ), Nusselt number (Nu), and Sherwood number (Sh) were analyzed at the annulus surfaces:

$$\tau_{0,1}=\left(\left(1+\frac{1}{\beta}\right)\frac{du}{d\xi}\right|_{\xi=0,1}, Nu_{0,1}=-\left(\frac{dv}{d\xi}\right|_{\xi=0,1}, Sh_{0,1}=-\left(\frac{dw}{d\xi}\right|_{\xi=0,1}. \tag{17}$$

3 | NUMERICAL SOLUTION

The controlling systems of Equations (11)–(14) are solved using CCA, due to global nature and its ability to handle systems of ODEs/PDEs, both nonlinear or linear equations.[30,40] The solution procedure includes assuming trial solutions as a sum of shifted Chebyshev basis ($G_i(\theta)$) for the unknown functions $u(\xi)$, $v(\xi)$, and $w(\xi)$. Generally, the Chebyshev basis function is defined on the interval $[-1, 1]$, and to utilize the technique, we introduced the mapping $\theta=2\xi-1$, such that the problem domain $\xi\in[0, 1]$ is transformed into $\theta\in[-1, 1]$ successfully. This numerical approach is fully documented in the studies of Akolade et al.,[34] Babatin,[41] Javed and Mustafa,[42] and Mallawi.[43]

We present the trial solutions as a sum of shifted Chebyshev basis function $G_i(2\xi-1)$ associated with constants m_i, n_i, q_i to be determined as the unknown coefficients of velocity, temperature, and concentration, respectively;

$$u(\xi)=\sum_{i=0}^{P} m_i G_i(2\xi-1),\ v(\xi)=\sum_{i=0}^{P} n_i G_i(2\xi-1),\ \ w(\xi)=\sum_{i=0}^{P} q_i G_i(2\xi-1) \tag{18}$$

Substituting Equation (18) into Equation (14), the boundary conditions give the following sets of algebraic equation:

$$\begin{gathered}\left[\sum_{i=0}^{P} m_i G_i(2\xi-1)-\left(1+\frac{1}{\beta}\right)\beta_v kn\frac{d}{d\xi}\sum_{i=0}^{P} m_i G_i(2\xi-1)\right]_{\xi=0}=0,\\ \left[\sum_{i=0}^{P} n_i G_i(2\xi-1)-1-S\beta_v kn\frac{d}{d\xi}\sum_{i=0}^{P} n_i G_i(2\xi-1)\right]_{\xi=0}=0,\left[\sum_{i=0}^{P} q_i G_i(2\xi-1)-1\right]_{\xi=0}=0,\\ \left[\sum_{i=0}^{P} m_i G_i(2\xi-1)+\left(1+\frac{1}{\beta}\right)\beta_v kn\frac{d}{d\xi}\sum_{i=0}^{P} m_i G_i(2\xi-1)\right]_{\xi=1}=0,\\ \left[\sum_{i=0}^{P} n_i G_i(2\xi-1)+S\beta_v kn\frac{d}{d\xi}\sum_{i=0}^{P} n_i G_i(2\xi-1)\right]_{\xi=1}=0,\left[\sum_{i=0}^{P} q_i G_i(2\xi-1)-Rc\right]_{\xi=1}=0.\end{gathered} \tag{19}$$

Substituting Equation (18) into the transformed systems (11)–(13), residues $R_U(\xi, m_i, n_i, q_i)$, $R_V(\xi, m_i, n_i, q_i)$, and $R_W(\xi, n_i, q_i)$ are generated and minimized close to zero via collocation techniques[34,41-43]:

$$\text{for } \delta(\xi-\xi_j)=\begin{Bmatrix}1, \xi=\xi_j\\ 0, \text{otherwise}\end{Bmatrix}, \tag{20}$$

$$\begin{gathered}\int_0^L R_U(\xi, m_i, n_i, q_i)d\xi = R_U(\xi, m_i, n_i, q_i)=0, \int_0^L R_V(\xi, m_i, n_i, q_i)d\xi = R_V(\xi, m_i, n_i, q_i)\\ =0, \int_0^L R_W(\xi, n_i, q_i)d\xi = R_W(\xi, n_i, q_i)=0, \text{for j}=1, 2, ..., N-1\end{gathered} \tag{21}$$

where η_j denotes the shifted Gauss–Lobatto collocation points defined as

$$\xi_j=\frac{1}{2}\left(1-\cos\left(\frac{j\pi}{N}\right)\right), for\ j=0, 1, ..., N. \tag{22}$$

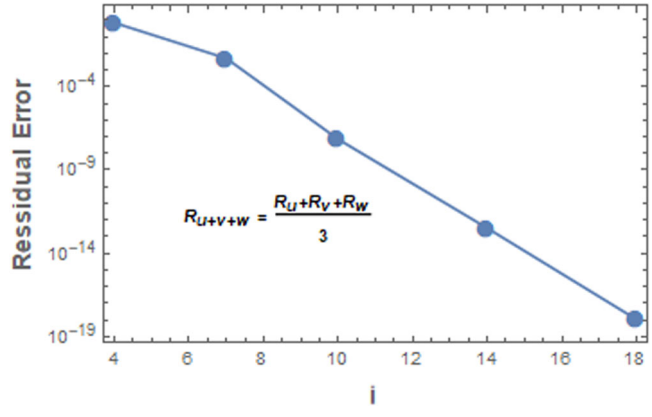


FIGURE 2 The minimized residual error [Color figure can be viewed at wileyonlinelibrary.com]

TABLE 1 Comparison of $u(\xi)$ and $v(\xi)$ at $Nc = \gamma = \alpha = s_1 = s_2 = Ec = Nb = Nt = Nc = 0, \eta = 8$, $\beta \to Da \to 0$ for different values of $\beta_v kn$ and ξ

Values		Velocity profile $u(\xi)$		Temperature profile $v(\xi)$	
$\beta_v kn$	ξ	Jha et al.[8]	Present	Jha et al.[8]	Present
0.0	0.2	0.0460	0.0459751	0.7814	0.781351
	0.5	0.0576	0.0575799	0.4722	0.472165
	0.7	0.0409	0.0409420	0.2773	0.277290
	0.9	0.0145	0.0145276	0.0905	0.090537
0.01	0.2	0.0484	0.0484402	0.7706	0.770565
	0.5	0.0597	0.0597107	0.4713	0.471277
	0.7	0.0430	0.0429837	0.2826	0.282641
	0.9	0.0136	0.0162941	0.1019	0.101867
0.1	0.2	0.0690	0.069037	0.6976	0.697619
	0.5	0.0786	0.0785501	0.4653	0.465275
	0.7	0.0616	0.0615907	0.3188	0.318833
	0.9	0.0334	0.0334419	0.1785	0.178494

TABLE 2 Computational values for Skin friction coefficient (τ) for different values of Da, β,s_1, s_2, and η

η	s_1	τ_0	τ_1	s_1	τ_0	τ_1	β	τ_0	τ_1	Da	τ_0	τ_1
0.2	0.5	0.79009	0.37183	0.5	0.69830	0.33186	0.1	0.70757	0.39447	1	0.71022	0.31561
	1.0	0.82406	0.3833	1.0	0.82406	0.38330	0.3	0.88425	0.37517	5	0.82406	0.38330
	1.5	0.85826	0.39487	1.5	0.94795	0.43375	0.5	0.94621	0.36564	10	0.84131	0.39366
0.5	0.5	0.74662	0.42585	0.5	0.68091	0.39149	0.1	0.72330	0.46394	1	0.69021	0.36903
	1.0	0.79444	0.44735	1.0	0.79444	0.44735	0.3	0.82774	0.43690	5	0.79444	0.44735
	1.5	0.84266	0.46909	1.5	0.90668	0.50229	0.5	0.85991	0.42542	10	0.81012	0.45928
0.8	0.5	0.73958	0.46904	0.5	0.68509	0.43889	0.1	0.74075	0.51625	1	0.69192	0.41079
	1.0	0.79498	0.49851	1.0	0.79498	0.49851	0.3	0.81934	0.48748	5	0.79498	0.49851
	1.5	0.85088	0.52834	1.5	0.90375	0.55722	0.5	0.84237	0.47550	10	0.81045	0.51185

TABLE 3 Computational values for Heat transfer coefficients (Nu) for different values of η, Nt, Nb, Pr, and Ec

η	Nt	Nu_0	Nu_1	Nb	Nu_0	Nu_1	Pr	Nu_0	Nu_1	Ec	Nu_0	Nu_1
0.2	0.1	1.60675	0.55724	0.1	1.60675	0.55724	1	1.83473	0.45831	0.1	1.66612	0.51701
	0.3	1.53057	0.59895	0.3	1.54701	0.57408	3	1.75011	0.49485	0.3	1.64903	0.52859
	0.5	1.4574	0.64011	0.5	1.48158	0.59618	6	1.61602	0.55318	0.5	1.63205	0.54010
0.5	0.1	0.86882	0.82744	0.1	0.86882	0.82744	1	1.09494	0.69380	0.1	0.92495	0.77930
	0.3	0.82475	0.86516	0.3	0.82432	0.85912	3	1.01068	0.74318	0.3	0.90885	0.79312
	0.5	0.78451	0.90137	0.5	0.78003	0.89232	6	0.87796	0.82197	0.5	0.8928	0.80688
0.8	0.1	0.61368	1.02558	0.1	0.61368	1.02558	1	0.84411	0.86519	0.1	0.67097	0.97083
	0.3	0.58392	1.06057	0.3	0.57359	1.06803	3	0.75819	0.92442	0.3	0.65456	0.98651
	0.5	0.55607	1.09542	0.5	0.53648	1.1094	6	0.62299	1.01901	0.5	0.63818	1.00217

TABLE 4 Computational values for Sherwood number (Sh) for different values of η, Nt, Nb, and Rc

η	Nt	Sh_0	Sh_1	Nb	Sh_0	Sh_1	Rc	Sh_0	Sh_1
0.2	0.1	0.89433	0.62268	0.1	0.89433	0.62268	0.1	1.14492	0.67547
	0.3	−0.68887	0.897192	0.3	1.68332	0.46405	0.2	0.89433	0.62268
	0.5	−1.53377	0.938066	0.5	1.84197	0.43096	0.3	0.64577	0.56883
0.5	0.1	1.11391	0.626783	0.1	1.11391	0.62678	0.1	1.25882	0.70019
	0.3	1.33729	0.522382	0.3	1.17523	0.57494	0.2	1.11391	0.62678
	0.5	1.9096	0.147723	0.5	1.18666	0.56373	0.3	0.97006	0.55254
0.8	0.1	1.13073	0.58606	0.1	1.13073	0.58606	0.1	1.24264	0.67576
	0.3	1.80094	0.09974	0.3	1.00038	0.64710	0.2	1.13073	0.58606
	0.5	2.7115	−0.70129	0.5	0.97297	0.65893	0.3	1.01958	0.49562

Following this procedure, the $3P + 3$ unknown coefficients m_i, n_i, q_i are obtained. A system of $3P + 3$ algebraic equations is formed. The Newton method is employed to solve the algebraic equations. All the computation in this study is carried out with the help of Mathematical symbolic package MATHEMATICA 11.3. We present the computational

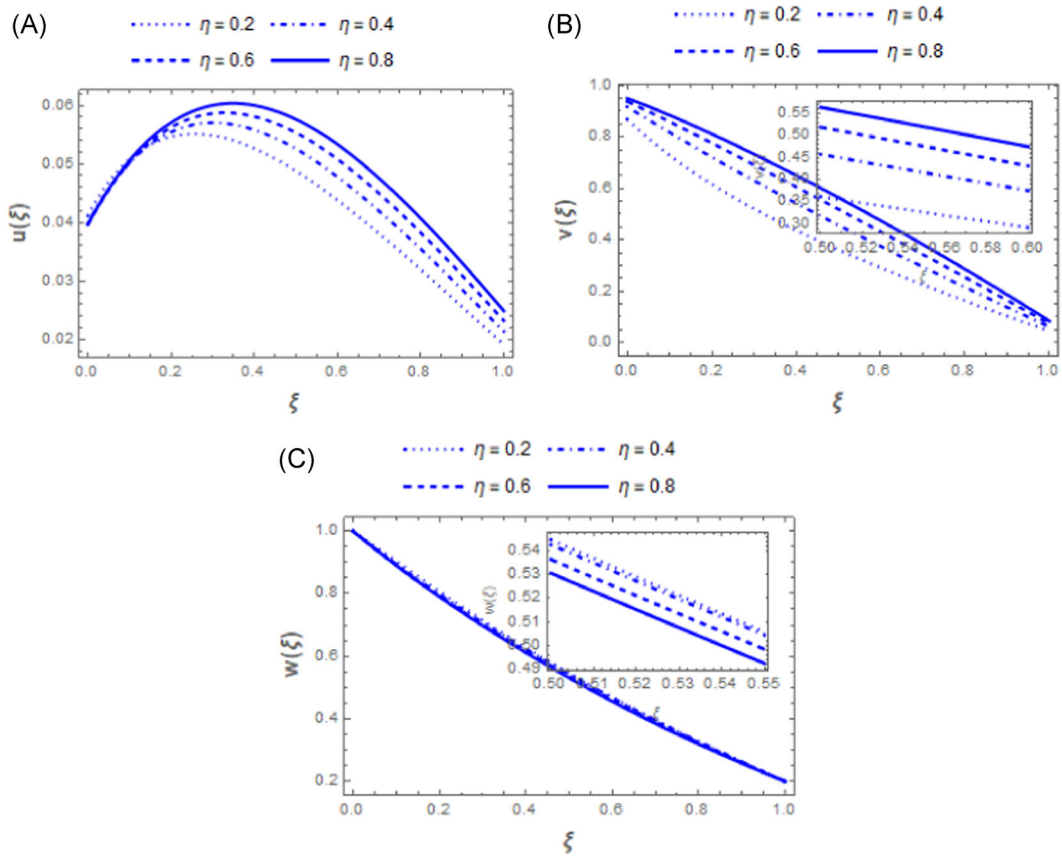


FIGURE 3 The impact of the radii ratio (η) on (A) $u(\xi)$ (B) $v(\xi)$, and (C) $w(\xi)$ profiles [Color figure can be viewed at wileyonlinelibrary.com]

graph of the total average square residual error of the flow distributions $u(\xi)$, $v(\xi)$, and $w(\xi)$ (see Figure 2).

4 | RESULTS AND DISCUSSION

In this study, the nonlinear convection flow of a dissipative Casson nanofluid through an inclined annular microchannel with a porous medium is analyzed. The momentum, temperature, nanoparticle volume fraction, volumetric flow rate, skin friction, and rate of heat and mass transfer at both surfaces are computed and tabled for constant values of $\alpha = 0.1, \gamma = \frac{\pi}{3}, s_1 = s_2 = 1, Nc = 2, Da = 5, Nt = Nb = Ec = 0.1, \beta_v kn = 0.05, S = 1.64, Pr = 6.2, Ha = 0.5, \beta = 0.2, Rc = 0.2, \eta = 0.5$, following Oni and Jha,[7] Jha et al.,[8] and Gireesha and Roja[39] throughout the investigation, else otherwise stated. Table 1 presents the accuracy and efficiency of the numerical method used, compared with the existing work of Jha et al.,[8] and the results were in conformity. Tables 2–4 present the effects of pertinent parameters on skin friction coefficient, Nusselt number, and Sherwood number, respectively, at

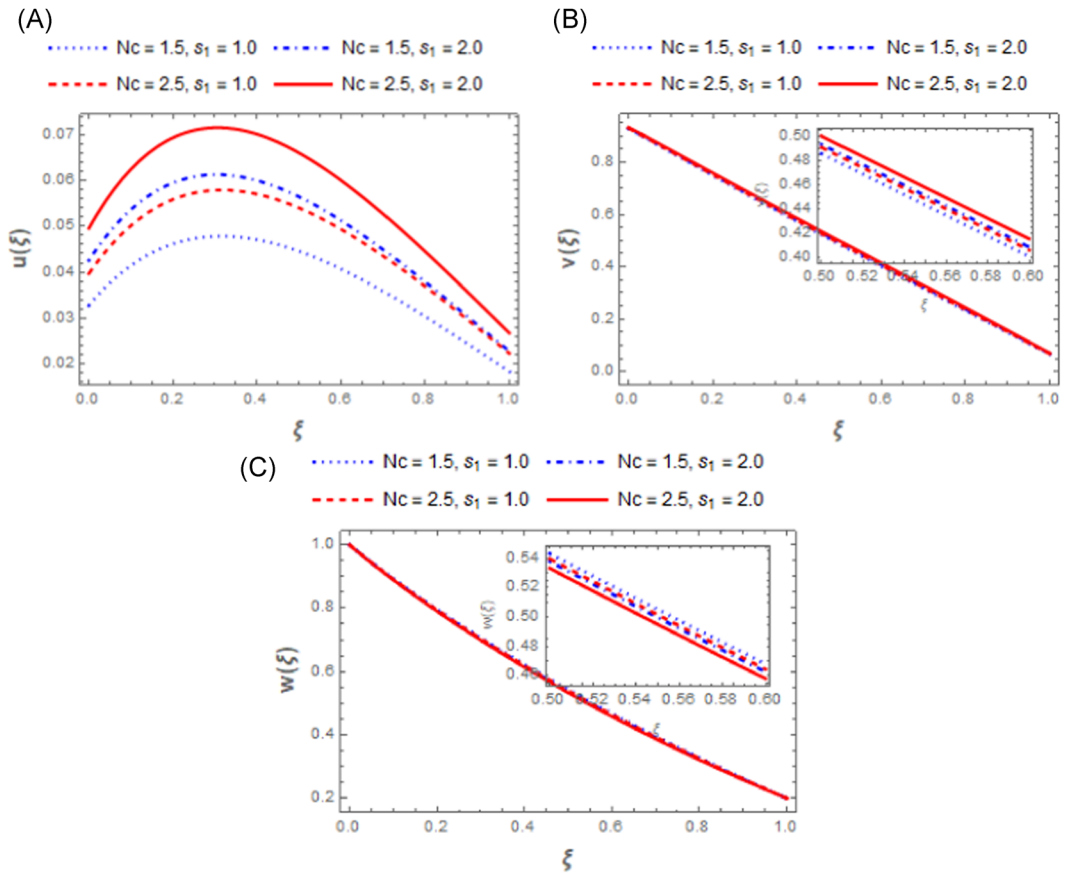


FIGURE 4 The impact of the buoyancy ratio (Nc) and nonlinear thermal convection (s_1) on (A) $u(\xi)$, (B) $v(\xi)$, and (C) $w(\xi)$ profiles [Color figure can be viewed at wileyonlinelibrary.com]

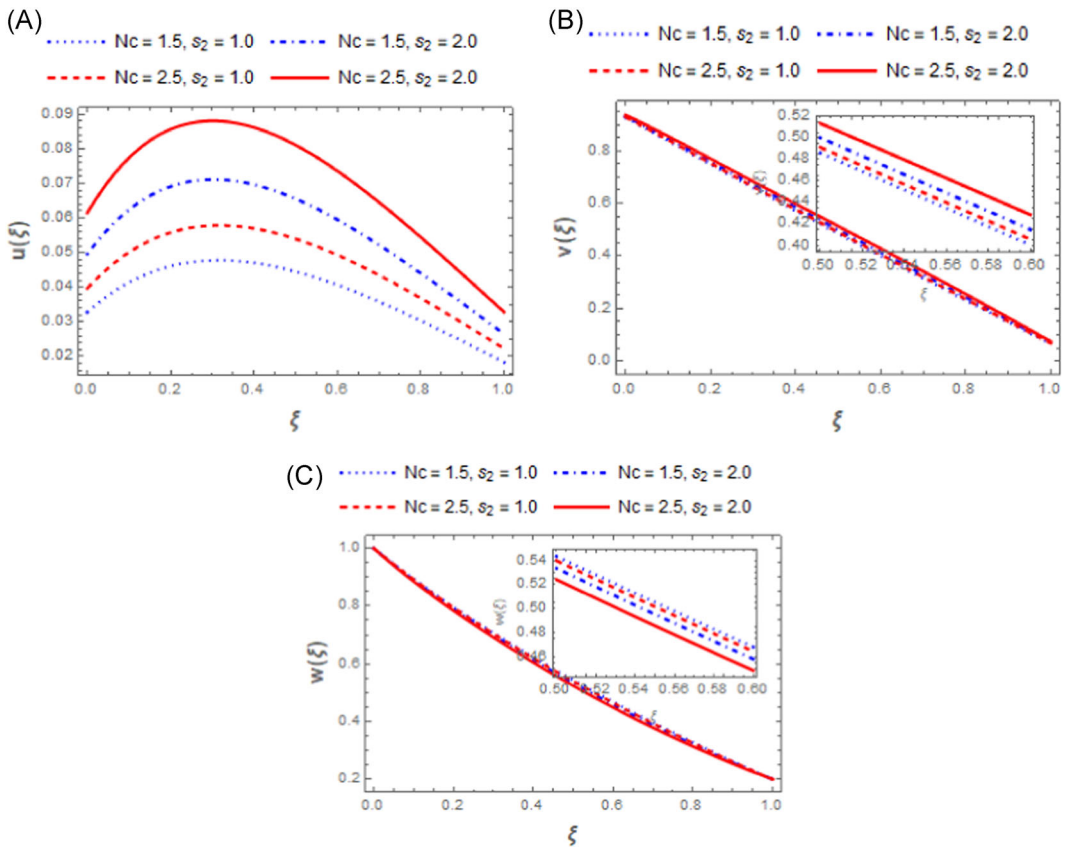


FIGURE 5 The impact of the buoyancy ratio (Nc) and nonlinear solutal convection (s_2) on (A) $u(\xi)$, (B) $v(\xi)$, and (C) $w(\xi)$ profiles [Color figure can be viewed at wileyonlinelibrary.com]

both cylinder surfaces. Figures 3–10 depict the graphical interpretation of flow parameters through the annular gap.

Figure 3A–C present the effect of radii ratio parameter (η) on dimensionless profiles $u(\xi)$, $v(\xi)$, and $w(\xi)$ across the annular medium. Physically, the wider flow region gives room for free movement of fluid particles and allows them to gain more energy via collision with each other and the walls, thereby reducing the cohesive force between the fluid particles, which results in a lower fluid concentration. It is evident from Figure 3A,B that the velocity and temperature profiles are elevated with a wider annular gap ratio, whereas a decrease is noticed in the concentration profile (see Figure 3C). More important, an increase in the curvature radius ratio increased the temperature at both surfaces, and it is observed to increase the velocity slip at $\xi = 1$ and decrease it at $\xi = 0$.

The effect of buoyancy ratio (Nc), nonlinear thermal convection (s_1), and nonlinear solutal convection (s_2) on dimensionless profiles $u(\xi)$, $v(\xi)$, and $w(\xi)$ across the annular gap is presented in Figures 4 and 5, accordingly. The fluid velocity and temperature increase with an increase in Nc, s_1, and s_2, as shown in Figures 4A,B and 5A,B, respectively. However, a decreasing behavior of nanoparticle volume fraction profile is realized for the increase in these parameters (see Figures 4C and 5C). Physically, the convection effect is known to exert buoyancy forces on the flow region, which, in turn, intensifies the fluid flow distributions, as we

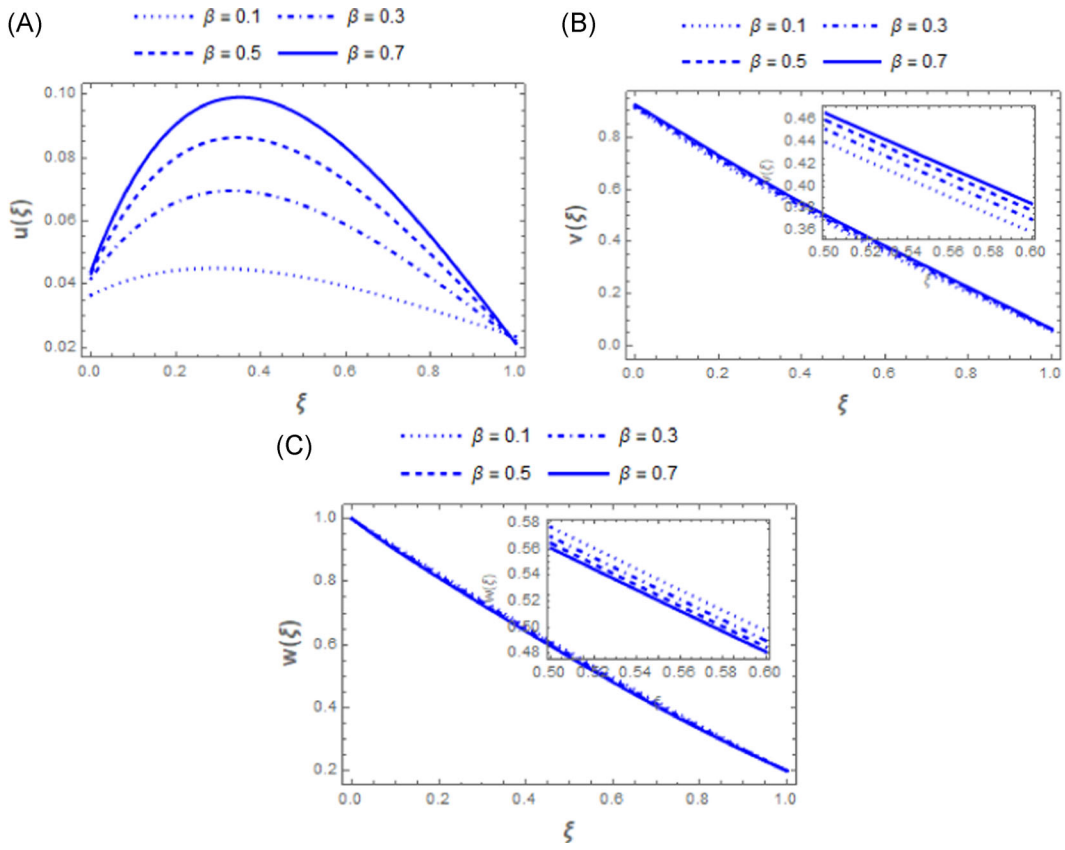


FIGURE 6 The impact of Casson (β) on (A) $u(\xi)$, (B) $v(\xi)$, and (C) $w(\xi)$ profiles [Color figure can be viewed at wileyonlinelibrary.com]

can see in the respective figures. It is worth mentioning that the solutal convection parameter impacted $u(\xi)$, $v(\xi)$, and $w(\xi)$ profiles significantly, compared with the thermal convection, both at the annular gap and at the cylinder surfaces.

The variation in $u(\xi)$, $v(\xi)$, and $w(\xi)$ corresponding to higher values of the Casson parameter (β) is pictured in Figures 6A–C. Evidently, in Figures 6A,B, fluid momentum and energy get accelerated with a continuous increase of β, whereas Figure 6C shows a decrease in nanoparticle volume fraction with a rise in β. Physically, as $\beta \to \infty$, the fluid neutralizes itself from non-Newtonian to Newtonian category. Thus, larger β leads to boundary layer enhancement, hence leading to the respective results (see Figures 6A–C).

Figures 7A–C describe the influence of thermophoresis (Nt) and Brownian motion (Nb) on $u(\xi)$, $v(\xi)$, and $w(\xi)$ profiles, accordingly, through the annular medium. Multiple values of Nb entirely promote the energy, momentum, and nanoparticle volume fraction profiles, whereas a continuous increase of Nt decelerates both velocity and concentration profiles, but increases the fluid temperature within the annular region. It is worth noting that the continuous collision of nanoparticles generates thermal energy, coupled with the particle movement from a higher temperature region to a lower region, which increases the fluid temperature (see Figure 7B). The movement of nanoparticles away from the cylinder surfaces resulted in a decrease of nanoparticle volume fraction and slip effects with an increase in Nt (see Figure 7C).

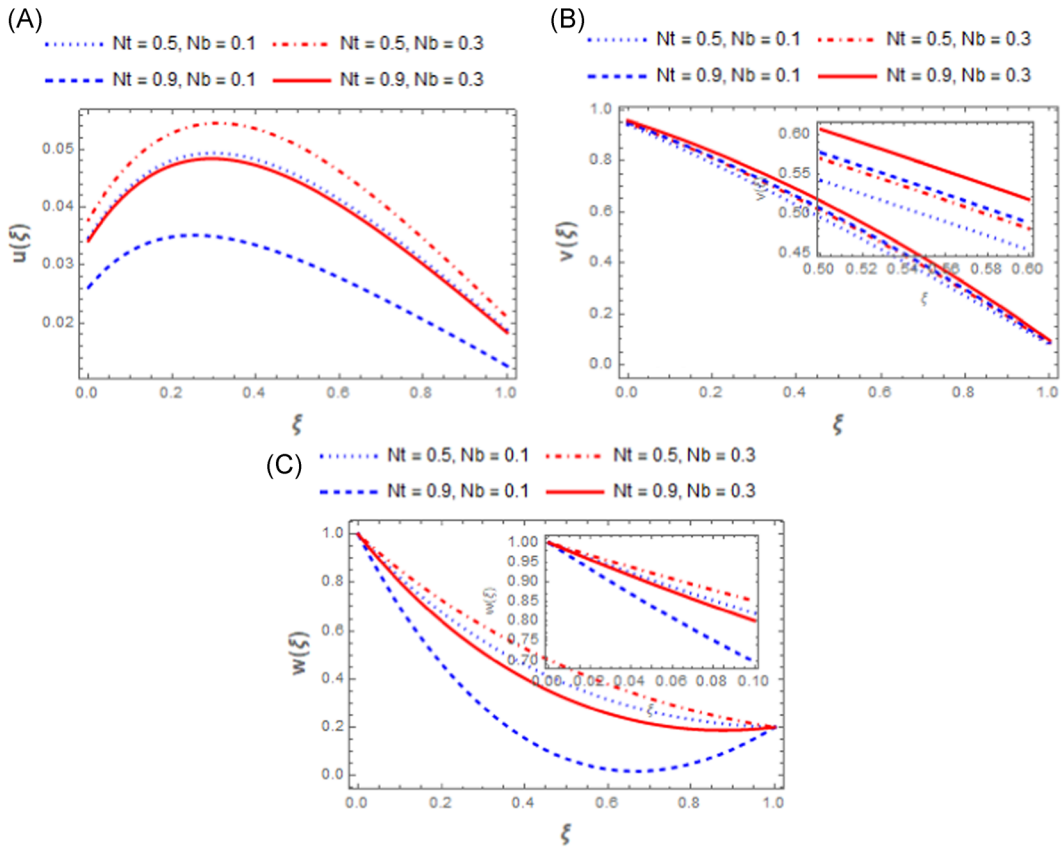


FIGURE 7 The impact of thermophoresis (Nt) and Brownian motion (Nb) on (A) $u(\xi)$, (B) $v(\xi)$, and (C) $w(\xi)$ profiles [Color figure can be viewed at wileyonlinelibrary.com]

The effect of the heat source (α) and Prandtl number (Pr) on $u(\xi)$, $v(\xi)$, and $w(\xi)$ profiles is reported in Figure 8A–C, accordingly. The higher magnitude of α is seen to diminish (a decrease that is attributed to reduced thicknesses of solutal and thermal boundary layer, i.e., thermal diffusivity factor) both nanoparticle volume fraction and velocity, and increase the temperature fields in the process. The same results are, however, seen for a large value of Prandtl number. Higher quality products can be obtained in coiling industries with the well-calculated Prandtl number.

The impact of magnetic field (Ha) and inclination angle (γ) is perceived in Figure 9A–C on the flow profiles $u(\xi)$, $v(\xi)$, and $w(\xi)$, accordingly. It is observed from Figure 9A,B that the velocity and temperature diminish with an increase in parameters Ha and γ. This is due to the Lorentz force generated by the impact of the magnetic field in an electrically conducting fluid, which acts in the direction opposite of the flow, causing a flow retardation effect that tends to decrease the fluid velocity. Also, a decrease in fluid nanoparticle volume fraction is observed with an increase in Ha and γ, as shown in Figure 9C.

The analysis of various pertinent parameters at per unit time of fluid passing through a system (the flow volumetric rate) is presented in Figure 10A,B, where large porosity medium, higher solutal and thermal convection, enhanced Casson parameter, and wider annular gap

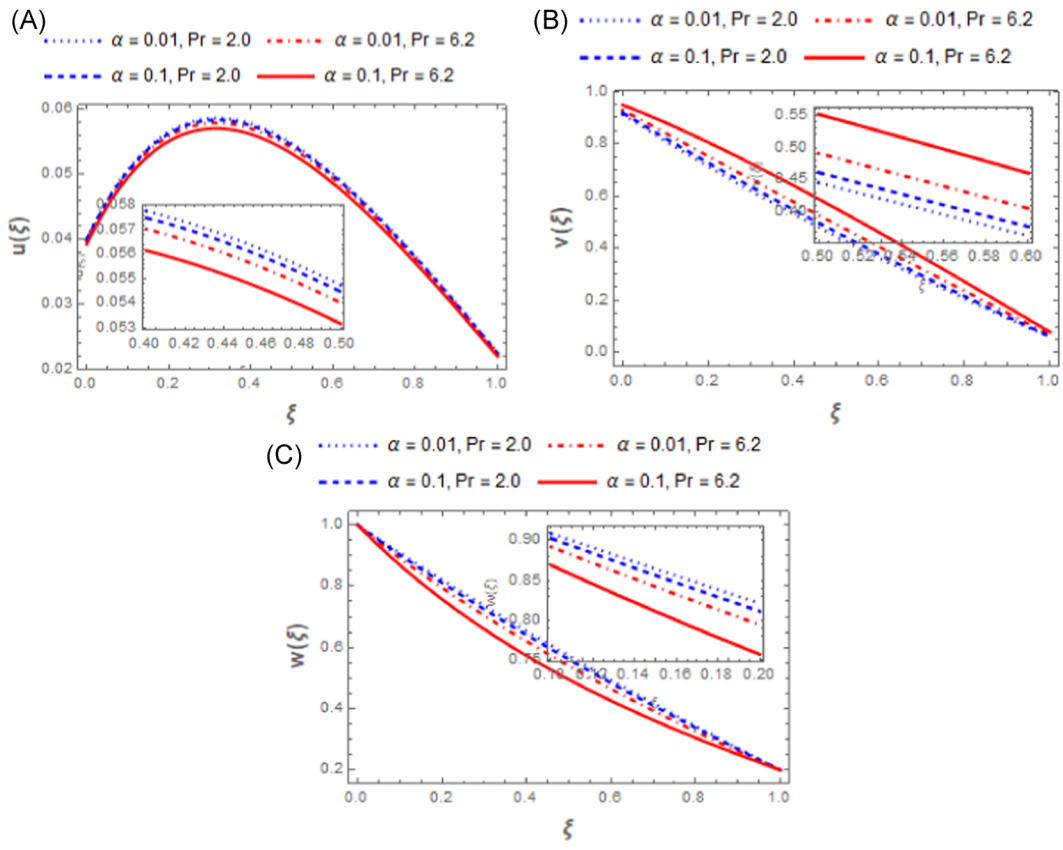


FIGURE 8 The impact of heat generation (α) and Prandtl number (Pr) on (A) $u(\xi)$, (B) $v(\xi)$, and (C) $w(\xi)$ profiles [Color figure can be viewed at wileyonlinelibrary.com]

signify a great enhancement in the fluid flow rate across the flow region, except the inclination angle, which is observed to exhibit an opposite behavior.

Critical investigations on skin friction coefficient, heat transfer coefficient, and Sherwood number are presented in Tables 2–4, respectively, for the effects of radii ratio, nonlinear thermal and solutal number, Casson, porosity, Prandtl number, thermophoresis, Brownian motion, Eckert number, and wall concentration ratio at both cylinder surfaces.

5 | CONCLUSIONS

Investigations of the impact of Brownian motion, magnetic field, and thermophoresis features on the motion of dissipative Casson fluid flowing through an inclined annular cylinder with a porous medium and nonlinear convection process are carried out and discussed. The governing fully developed nonlinear flow regime of an electrically conducting fluid is nondimensionalized and solved for flow distributions and physical quantities using CCA. The following findings are made:

1. A continuous increase of β rendered this flow model into a Newtonian fluid.

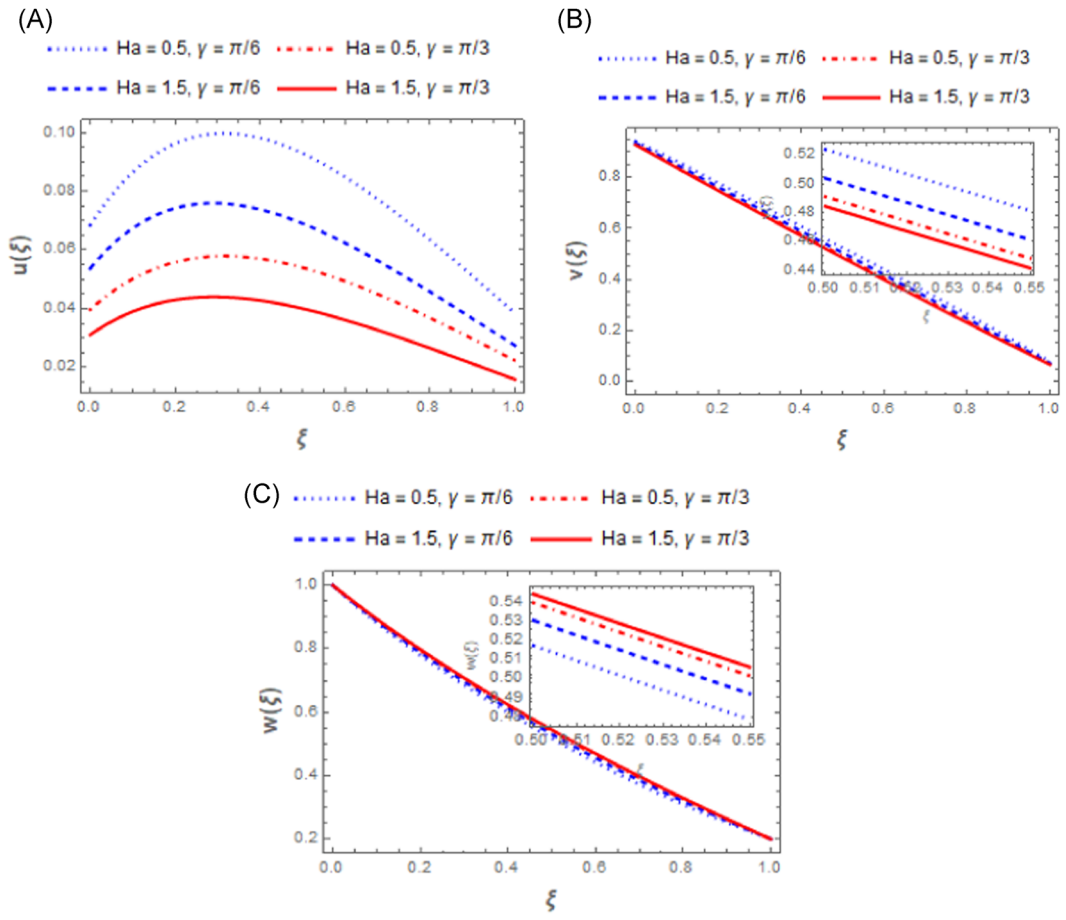


FIGURE 9 The impact of magnetic field (Ha) and inclination angle (γ) on (A) $u(\xi)$, (B) $v(\xi)$, and (C) $w(\xi)$ profiles [Color figure can be viewed at wileyonlinelibrary.com]

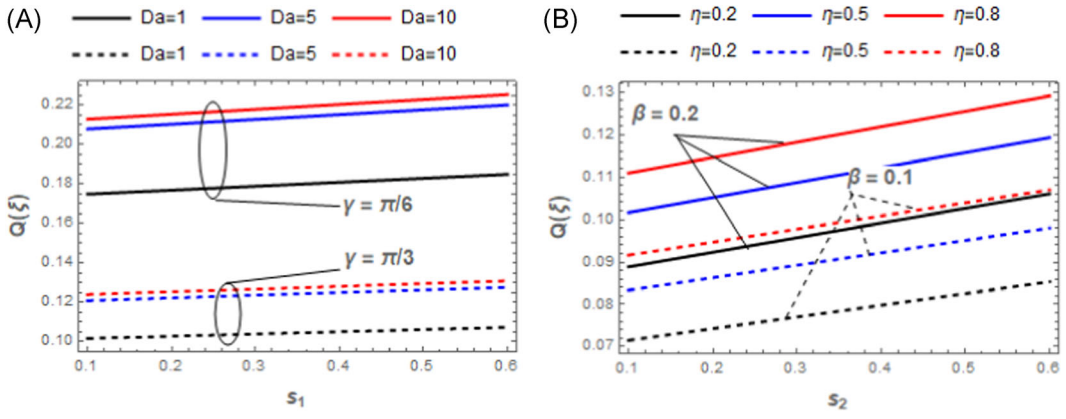


FIGURE 10 The impact of γ, Da, β, s_1, s_2, and η on the volumetric flow rate $Q(\xi)$ [Color figure can be viewed at wileyonlinelibrary.com]

2. A hike in s_1 and s_2 corresponds to an increase in velocity and temperature profiles, whereas it decreases the nanoparticle volume fraction.
3. An increase in solutal and thermal convection, Casson parameter, wider porosity medium, and annular gap signifies a great enhancement in the fluid flow rate across the flow region.
4. Increasing values of the Hartman number and inclination angle pronounce the nanoparticle volume fraction but decreases both temperature and velocity fields.
5. CCA exhibited enough accuracy and efficiency, with less computational time.
6. A rise in η increases the temperature at both surfaces, increases the velocity slip at $\xi = 1$, and decreases the velocity slip at $\xi = 0$.
7. The thermophoresis parameter is seen to increase all the fluid distributions positively across the annular gap.

Microfluidics, basically product miniaturization, that is, the dynamics of assessing and controlling the fluid behavior through a microchannel, is seen as a reducing mechanism in the production of devices and is an enhancing factor of thermal energy. This system is found applicable in the micro heat exchanger, cooling of store grain, a geothermal system usage, oil extraction, groundwater pollution, storage of nuclear wastes, MHD micropumps, thermal insulation multidisciplinary fields, among others. Concerning this, investigations into the nonlinear convection flow process of a nanofluid in an annular microchannel with a porous medium become imperative, as they will aid understanding of the flow process and assist industrial applications for better performance. More studies could include investigation into different fluid rheology and analysis of the fluid thermophysical properties for proper flow prediction (to achieve a remarkable convection process).

NOMENCLATURE

Nc	buoyancy ratio
B_0	magnetic flux density
c_p	specific heat at constant pressure
β_t, β_v	dimensionless parameter
D^*	mass diffusivity
γ_a	ratio of specific heat
β	Casson parameter
ς_d	molecular mean free path
α	generation/absorption
V_o	temperature at the inlet
Kn	Knudsen number
γ	inclination angle
Ha	Hartman number
s_1	nonlinear thermal convection
Nu	heat transfer coefficient
s_2	nonlinear solutal convection
S	wall–fluid interaction
ρ_0	fluid mixture density
Pr	Prandtl number
ν_0	kinematic viscosity
η	radii ratio parameter
k_0	thermal conductivity

W_o concentration at the inlet
ρ fluid density
c_1, c_2 inner and outer cylinders radius
σ_v thermal accommodation
Rc wall concentration ratio
σ_t tangential momentum accommodation
W_1 outer–inner surface concentration
v dimensionless temperature
Sh Sherwood number
w dimensionless concentration
V fluid temperature
W_2 inner–outer surface concentration
V_2 inner–outer surface temperature
W fluid concentration
V_1 outer–inner surface temperature
u dimensionless axial velocity
u dimensional axial velocity
t dimensional radial coordinates
ξ dimensionless radial coordinate
δ dimensionless gap between the cylinders

ORCID

Mojeed T. Akolade https://orcid.org/0000-0002-6876-7203

REFERENCES

1. Akbar MZ, Ashraf M, Iqbal MF, Ali K. Heat and mass transfer analysis of unsteady MHD nanofluid flow through a channel with moving porous walls and medium. *AIP Adv*. 2016;6:045222. https://doi.org/10.1063/1.4945440
2. Girish N, Sankar M, Makinde OD. Developing buoyant convection in vertical porous annuli with unheated entry and exit. *Heat Transfer*. 2020;49(5):2551-2576. https://doi.org/10.1002/htj.21734
3. Lawal KK, Jibril HM. Impact of relative motion of a magnetic field on unsteady magnetohydrodynamic natural convection flow with a constant heat source/sink. *Heat Transfer*. 2020. https://doi.org/10.1002/htj.21888
4. Panigrahi L, Panda J, Kumar D, Sahoo SS. Analytical investigation of polar fluid flow with induced magnetic field in concentric annular region *Heat Transfer*. 2020;49(6):3943-3957. https://doi.org/10.1002/htj.21816
5. Anurag, Singh AK, Chandran P, Sacheti NC. Effect of Newtonian heating/cooling on free convection in an annular permeable region in the presence of heat source/sink. *Heat Transfer*. 2020. https://doi.org/10.1002/htj.21900
6. Jha BK, Joseph S, Ajibade A. Role of thermal diffusion on double-diffusion natural convection in a vertical annular porous medium. *Ain Sham Eng J*. 2015;6(2):629-637.
7. Oni M, Jha BK. Heat generation/absorption effects on material convection flow in a vertical annulus with time-periodic boundary conditions. *J Aircraft Spacecraft Technol*. 2019;3:183-196.
8. Jha BK, Aina B, Isa S. Fully developed MHD natural convection flow in a vertical annular microchannel: an exact solution. *J King Saud Univ Sci*. 2015;27(3):253-259.
9. Yusuf T. Exact solution of an MHD natural convection flow in vertical concentric annulus with heat absorption. *Int J Fluid Mech Therm Sci*. 2017;3(5):52-61.
10. Jha BK, Yusuf TS. Transient-free convective flow with heat generation/absorption in an annular porous medium: a semi-analytical approach. *Proc Inst Mech Eng E*. 2018;232:1-14. https://doi.org/10.1177/0954408917730995

11. Isa S, Aina B, Jha BK, Makinde OD. Mixed convection flow behaviour in existence of lorentz forces in a vertical micro circular duct having time periodic boundary conditions: steady periodic regime. *J Pure Appl Sci*. 2020;20:137-149.
12. Gireesha BJ, Sindhu S. MHD natural convection flow of Casson fluid in an annular microchannel containing porous medium with heat generation/absorption. *Nonlinear Eng*. 2020;9:223-232. https://doi.org/10.1515/nleng-2020-0010
13. Thriveni K, Mahanthesh B, Lorenzini G, Animasaun IL. Significance of induced magnetic field and exponential space dependent heat source on quadratic convective flow of Casson fluid in a micro-channel via HPM. *Math Model Eng Probl*. 2019;6(3):369-384.
14. Mahanthesh B, Brizlyn T, Shehzad S, B.J.G. Nonlinear thermo-solutal convective flow of Casson fluid over an oscillating plate due to non-coaxial rotation with quadratic density fluctuation: exact solutions. *Multidiscip Model Mater Struct*. 2019;15(4):818-842. https://doi.org/10.1108/MMMS-06-2018-0124
15. Pantzali MN, Mouza AA, Paras SV. Investigating the efficacy of nanofluids as coolants in plate heat exchangers (PHE). *Chem Eng Sci*. 2009;64:3290-3300.
16. Hamad MA, Pop I. Scaling transformations for boundary layer flow near the stagnation-point on a heated permeable stretching surface in a porous medium saturated with a nanofluid and heat generation/absorption effects. *Transp Porous Media*. 2010;87:25-39.
17. Pal D, Mandal G. Mixed convection-radiation on stagnation-point flow of nanofluid over a stretching shrinking sheet in a porous medium with heat generation and viscos dissipation. *J Petrol Sci Eng*. 2015;126:16-25.
18. Gyatri M, Jayaramireddy K, Babu MJ. Nonlinear convective flow of Maxwell fluid over a slandering stretching sheet with heat source/sink. *J Appl Comput Mech*. 2019. https://doi.org/10.22055/JACM.2019.31394.1868
19. Kumar R, Sood S. Interaction of magnetic field and nonlinear convection in the stagnation point flow over a shrinking sheet. *J Eng*. 2016;2016:6752520. https://doi.org/10.1155/2016/6752520
20. Thriveni K, Mahanthesh B. Nonlinear Boussinesq buoyancy driven flow and radiative heat transport of magnetohybrid nanoliquid in an annulus: a statistical framework. *Heat Transfer*. 2020;49(8):4759-4782. https://doi.org/10.1002/htj.21851
21. Thriveni K, Mahanthesh B. Optimization and sensitivity analysis of heat transport of hybrid nanoliquid in an annulus with quadratic Boussinesq approximation and quadratic thermal radiation. *Eur Phys J Plus*. 2020;135:459. https://doi.org/10.1140/epjp/s13360-020-00484-8
22. Hayat T, Qayyum S, Alsaedi A. Mechanisms of nonlinear convective flow of jeffrey nanofluid due to nonlinear radially stretching sheet with convective conditions and magnetic field. *Results Phys*. 2017;7:2341-2351.
23. Wubshet I, Dachasa G. Nonlinear convection flow of Williamson nanofluid past a radially stretching surface. *AIP Adv*. 2019;9:085026. https://doi.org/10.1063/1.5113688
24. Adesanya SO, Ogunseye HA, Lebelo RS, Moloi KC. Second law analysis for nonlinear convective flow of a reactive couple stress fluid through a vertical channel. *Heliyon*. 2018;4:e00907.
25. Yusuf TA, Mamood F, Gbadeyan JA, Adesanya SO. Nonlinear convective flow of MHD Oldroyd 8-constant fluid in a chemical reaction and convective boundary condition. *J Therm Sci Eng*. 2020;12(5):051022.
26. Ibrahim W, Gizewu T. Nonlinear mixed convection flow of a tangent hyperbolic fluid with activation energy. *Heat Transfer*. 2020;49:2427-2448. https://doi.org/10.1002/htj21729
27. Hayat T, Qayyum S, Alsaedi, Ahmad B. Nonlinear convective flow with variable thermal conductivity and Cattaneo-Christov heat flux. *Neural Comput Appl*. 2017;31(1):295-305. https://doi.org/10.1007/s00521-017-3001.0
28. RamReddy CH, Naveen P, Srinivasacharya D. Nonlinear convective flow of non-Newtonian fluid over an inclined plate with convective surface condition; a Darcy-Forchheimer model. *Int J Appl Comput Math*. 2018;4(1):51. https://doi.org/10.1007/s40819-018-0484-z
29. Hayat T, Qayyum S, Alsaedi A. MHD nonlinear convective flow of Walters-B nanofluid over a nonlinear stretching sheet with variable thickness. *Int J Heat Mass Transf*. 2017;110:506-514.
30. Idowu AS, Akolade MT, Abubakar JU, Falodun BO. MHD free convective heat and mass transfer flow of dissipative Casson fluid with variable viscosity and thermal conductivity effects. *J Taibah Univ Sci*. 2020;14(1):851-862.

31. Alamri SZ, Khan AA, Azeez M, Ellahi R. Effects of mass transfer on MHD second grade fluid towards stretching cylinder: a novel perspective of Cattaneo-Christov heat flux model. *Phys Lett A*. 2019;383:276-281. https://doi.org/10.1016/j.physleta.2018.10.035
32. Elelamy AF, Elgazery NS, Ellahi R. Blood flow of MHD non-Newtonian nanofluid with heat transfer and slip effects: application of bacterial growth in heart valve. *Int J Numer Methods Heat Fluid Flow*. 2020;30(11): 4883-4908. https://doi.org/10.1108/HFF-12-2019-0910
33. Bhatti MM, Shahid A, Abbas T, Alamri SZ, Ellahi R. Study of activation energy on the movement of gyrotactic microorganism in a magnetized nanofluids past a porous plate. *Processes*. 2020;8:328.
34. Akolade M, Adeosun T, Olabode J. Influence of thermophysical features on MHD squeezed flow of dissipative Casson fluid with chemical and radiative effects. *J Appl Comput Mech*. 2020. https://doi.org/10.22055/jacm.2020.34909.2508
35. Aina B, Malgwi PB. MHD convection fluid and heat transfer in an inclined micro-porous channel. *Nonlinear Eng*. 2019;8:755-763. https://doi.org/10.1515/nleng.2018-0081
36. Yusuf TA, Adesanya SO, Gbadeyan JA. Entropy generation in MHD Williamson nanofluid over a convectively heated stretching plate with chemical reaction. *Heat Transfer*. 2020;49(4):1982-1999. https://doi.org/10.1002/htj.21703
37. Srinivasacharya D, Bindu KH. Entropy generation in a micro polar fluid flow through an inclined channel. *Alex Eng J*. 2016;55:973-982. https://doi.org/10.1016/j.aej.2016.02.027
38. Shriny A, Bayareh M, Nadooshan AA. Nanofluid flow in a microchannel with inclined cross-flow injection. *SN Appl Sci*. 2019;1(1):1015.
39. Gireesha BJ, Roja A. Second law analysis of MHD natural convection slip flow of Casson fluid through an inclined microchannel. *Multidiscip Model Mater Struct*. 2020;16(6):1435–1455. https://doi.org/10.1108/MMS.11.2019.0189
40. Kayvan S, Hadi H, Seyed-Mohammad T. Stagnation-point flow of upper-convected Maxwell fluids. *Int J Nonlinear Mech*. 2006;41:1242-1247.
41. Babatin MM. Numerical treatment for the flow of Casson fluid and heat transfer model over an unsteady stretching surface in the presence of internal heat generation/absorption and thermal radiation. *Appl Appl Math*. 2018;13(2):854-862.
42. Javed T, Mustafa I. Slip effect on a mixed convection flow of a third-grade fluid near the orthogonal stagnation point on a vertical surface. *J Appl Mech Tech Phys*. 2016;57(3):527-536.
43. Mallawi F. Application of a legendre collocation method to the space time variable fractional-order advection dispersion equation. *J Taibah Univ Sci*. 2019;13(1):324-330. https://doi.org/10.1080/16583655.2019.1576265

How to cite this article: Idowu AS, Akolade MT, Oyekunle TL, Abubakar JU. Nonlinear convection flow of dissipative Casson nanofluid through an inclined annular microchannel with a porous medium. *Heat Transfer*. 2020;1–19. https://doi.org/10.1002/htj.22033